ELSEVIER

Contents lists available at ScienceDirect

# Sensors and Actuators: B. Chemical

journal homepage: www.elsevier.com/locate/snb





# In vitro biosensing of $\beta$ -Amyloid peptide aggregation dynamics using a biological nanopore

Brian Lenhart <sup>a</sup>, Xiaojun Wei <sup>a,b</sup>, Brittany Watson <sup>b</sup>, Xiaoqin Wang <sup>a</sup>, Zehui Zhang <sup>b</sup>, Chen-zhong Li <sup>c</sup>, Melissa Moss <sup>a,b,\*</sup>, Chang Liu <sup>a,b,\*</sup>

- <sup>a</sup> Department of Chemical Engineering, University of South Carolina, Columbia, SC, 29208, USA
- <sup>b</sup> Biomedical Engineering Program, University of South Carolina, Columbia, SC, 29208, USA
- <sup>c</sup> Center for Cellular and Molecular Diagnostics, Department of Biochemistry and Molecular Biology, Tulane University School of Medicine, New Orleans, LA, 70112, IISA

### ARTICLE INFO

Keywords: Nanopore  $\alpha$ -hemolysin  $\beta$ -amyloid Aggregation Dynamics Biosensor

### ABSTRACT

Alzheimer's disease and other neurodegenerative disorders are becoming more prevalent as advances in technology and medicine increase living standards and life expectancy. Alzheimer's disease is thought to initiate development early in the patient's life and progresses continuously into old age. This process is characterized molecularly by the amyloid hypothesis, which asserts that self-aggregating amyloid peptides are core to the pathophysiology in Alzheimer's progression. Precise quantification of amyloid peptides in human bodily fluid samples (i.e. cerebrospinal fluid, blood) may inform diagnosis and prognosis, and has been studied using established biosensing technologies like liquid chromatography, mass spectrometry, and immunoassays. However, existing methods are challenged to provide single molecule, quantitative analysis of the disease-causing aggregation process. Ultra-sensitive nanopore biosensors can step in to fill this role as a dynamic mapping tool. The work in this paper establishes characteristic signals of  $\beta$ -amyloid 40 monomers, oligomers, and soluble aggregates, as well as a proof-of-concept foundation where a biological nanopore biosensor is used to monitor the extent of *in vitro*  $\beta$ -amyloid 40 peptide aggregation at the single molecule level. This foundation allows for future work to expand in drug screening, diagnostics, and aggregation dynamic experiments.

### 1. Introduction

The amyloid hypothesis argues Alzheimer's disease (AD) molecular pathophysiology is associated with two primary mechanisms: (1) the accumulation of insoluble neuronal cell surface deposits (senile plaques) - manifested via amyloid precursor protein (APP) cleavage to from  $\beta$ -amyloid peptides (A $\beta$ ) that then aggregate and subsequently precipitate onto the neuron surface; and (2) the accumulation of neurofibrillary tangles – via intracellular degradation of cytoskeletal elements that play a crucial role in maintaining structural integrity and support of the neuron [1]. The senile plaques negatively interfere with neurotransmitter transport, causing motor and sensory signal transmission inefficiencies. Neurofibrillary tangles describe neurons that have atrophied from their intracellular unraveling and are degenerating [2]. The phenotypical manifestation of these molecular phenomena is displayed in the plethora of AD symptoms: memory loss, difficulty forming new memories, difficulty completing familiar tasks, problems with

spoken and written word, confusion with time and location, and loss of fine motor dexterity [3]. Due to the progression of AD over one's lifetime, beginning as early as young adulthood, it is desirable to quantitatively study the aggregation of  $A\beta$  early in the patient's life to inform appropriate preventative actions or drug candidates to be explored.

 $A\beta$  is the natural molecular product from the turnover of neuronal transmembrane protein, amyloid precursor protein (APP) [4]. Due to the multiplicity in ways APP is enzymatically cleaved there exists a myriad of different sized  $A\beta$  peptides yielded, among which the most common peptides contain 40 and 42 amino acids – hence  $A\beta40$  and  $A\beta42$  nomenclature, respectively [5]. These peptides stoichiometrically aggregate into larger entities that range in size from soluble dimers and trimers (oligomers) to insoluble aggregates (fibrils) bearing numerous individually associated monomers [6]. The aggregation is a dynamic process that begins with the spontaneous self-association of  $A\beta$  monomers into oligomers, and then continues by the stoichiometric addition of monomers or other near-by aggregated oligomeric species to form

<sup>\*</sup> Corresponding authors at: Department of Chemical Engineering, University of South Carolina, Columbia, SC, 29208, USA. *E-mail addresses*: mossme@cec.sc.edu (M. Moss), changliu@cec.sc.edu (C. Liu).

larger, highly ordered, soluble aggregate species. An increasing body of evidence suggests that neuronal cell toxicity from A $\beta$  peptides is due to the presence of these intermediate sized, oligomeric and soluble A $\beta$  aggregates [7–9]. Although off-pathway oligomeric species are also produced due to imperfections in the aggregation process, these species do not yield higher ordered soluble or fibrillar species [10]. The end of the aggregation process is characterized by the presence of large, insoluble, fibrillar species that deposit between neurons *in vivo* as senile plaques (Fig. 1a).

Herein, we focus our attention on mapping the aggregation dynamics of  $A\beta$  peptides using a nanopore biosensor. Electrochemical nanopore systems made from pore-forming proteins have attracted tremendous attention in the biosensing field for their single-molecule sensitivity, reproducibility, robustness, and tailorable constituency [11]. The widely utilized protein nanopore,  $\alpha$ -hemolysin ( $\alpha$ HL), is a naturally occurring pore forming toxin secreted in monomer form by Gram-positive Staphylococcus aureus and preferentially oligomerizes into a heptamer on the surface of rabbit red blood cells, inducing cell lysis [12]. Biosensors based on  $\alpha HL$  have been applied to sequencing nucleic acids, characterizing functionalization or conformational changes of proteins, peptides, and polyelectrolytes, and detecting small molecules and ions [13–20]. The pore-forming protein,  $\alpha HL$ , has a sensing region of ~1.4 nm in diameter and can therefore translocate analytes with smaller dimensions from one side of the electrochemical cell to the other [21]. Species with a molecular diameter greater than 1.4 nm, although not able to translocate, can still interact with the nanopore to generate characteristic signals [22]. The AD Aβ40 peptide forms a natural hairpin from the hydrogen-bonded self-interactions of residues 18-26 with 31-40 [23]. This naturally increases the molecular diameter along the length axis of the polypeptide, effectively being folded in half. The consequence of this hairpin formation phenomena is observed in the output  $\alpha HL$  nanopore signal which is characterized by full ion exclusion from the nanopore sensing region during monomeric Aβ40 translocation. Due to the transit size limitations of the incredibly narrow  $\alpha HL$ , aggregate species any larger than the monomer are unable to transit the nanopore but, collectively, can produce a distinct signal identified as a bumping event.

The utility of  $\alpha$ HL is harnessed in this study to probe the aggregation dynamics of freshly purified AD associated A $\beta$ 40 monomer at different temperatures (4 °C and 37 °C) over a 20-day period. Nanopore signal characteristics involve observing current blockades (amount of electrolyte excluded from sensing region – I/I<sub>0</sub>) and dwell times (how long

the analyte interacts with the sensing region) of translocating and bumping species in solution [15,22,24]. This level of direct molecular quantification is not attainable with bulk spectroscopic, gel electrophoretic, or ELISA-based sensing techniques. Previous work on amyloid particle biosensing has been demonstrated using different nanopore configurations. Wang et al. have utilized biological nanopores for probing induced conformational changes imposed on A\u03c342 peptides by a known aggregation promoter (cyclodextrin) and a known aggregation inhibitor (Congo red) [25]. Houghtaling et al. have demonstrated the utility of lipid coated solid-state nanopore sensing of oligomeric species over a small size range, but the inherent complexity of solid-state nanopore systems compounded with the need to apply a lipid coating to reduce fouling of the solid-state membrane is not as straightforward or desirable for rapid and reproducible applications [5]. Yu et al. have utilized a confined glass solid-state nanopore system for the monitoring of  $A\beta42$  monomer, oligomer, and fibrillar species by establishing their characteristic signals [26]. While these studies represent significant advancement of nanopore-based amyloid peptide biosensing, there is still a need for the application of robust biological nanopores to identify different amyloid peptide species and to thoroughly understand the aggregation dynamics of Aβ40 over time and at different temperatures. The results from this study demonstrate the ability of  $\alpha HL$  nanopore to play a role in the detection of AD associated peptides and monitoring the chaotic oligomer reordering process of aggregating Aβ40 along the AD progression pathway through observing and quantifying single molecule interactions directly. Additionally, due to the extreme sensitivity of the nanopore system, there is a great potential for clinical uses. The proof-of-concept experimenting in this paper lays the foundation for future, more comprehensive probing into early AD detection, drug screening, and fundamental studies in other dynamic peptide aggregating disorders.

### 2. Results and discussion

# 2.1. Establishing nanopore reference signals for $A\beta 40$ monomer, oligomer, and larger soluble aggregate

In a previous work,  $\alpha$ HL nanopores were employed to study A $\beta$ 42 peptide aggregation [25]. Here, we chose A $\beta$ 40 as the study model for two reasons: (1) it presents a bigger challenge for obtaining data on A $\beta$ 40 early aggregation dynamics as it does not form stable oligomers; (2) although the mechanics of aggregation between the two peptides are

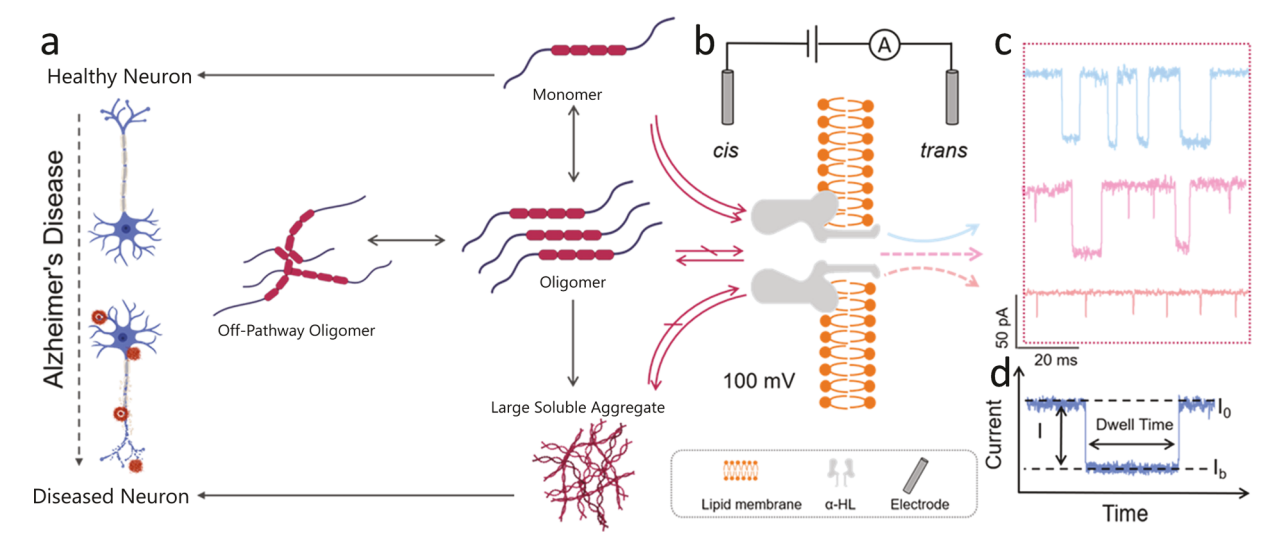


Fig. 1. a: Cellular and molecular schematic of AD progression from the amyloid aggregation perspective, juxtaposed with subsequent neuronal surface deposition. b: Interactions of various Aβ40 species with the  $\alpha$ HL nanopore. c: Characteristic signals of Aβ40 monomer (blue), oligomer (pink), and large soluble aggregate (orange) samples. d: Definition of nanopore sensor signal characteristics: current blockade (I/I<sub>0</sub>) and dwell time. (For interpretation of the references to colour in this figure legend, the reader is referred to the web version of this article.)

similar, Aβ40 has been demonstrated to aggregate over a longer time scale to allow for more insightful aggregation dynamics study [27]. To demonstrate that Aβ40 peptide aggregation dynamics can be visualized with higher resolution, reference signals must first be established using our nanopore biosensor. Monomeric Aβ40 species were isolated via size exclusion chromatography (SEC) purification (Figure S1). Oligomers were obtained by allowing monomer fractions to aggregate for 24 h [28]. When tested with a nanopore, these different aggregating molecular species produce distinct signal events due to various interactions with the pore (Fig. 1b). Monomeric Aβ40 peptide translocations through the  $\alpha HL$  nanopore exhibit long dwell times and full current blockades and are easily distinguishable from the brief, partial current blockades observed when oligomer or larger soluble aggregate entities bump into the pore and reverse back (Fig. 1c). The current blockade represents the capture of an individual molecule within the sensing region of the nanopore, which results in the exclusion of some current conducting ions and is mathematically defined as a relative dimensionless value to the open pore current (I/I<sub>0</sub>: I represents the current excluded from the nanopore by a translocating analyte, and I<sub>0</sub> represents the average baseline current through a stable open nanopore when no analyte is present). The dwell time signifies the amount of time an analyte occupies the sensing region of the nanopore and implies the effective interaction between the nanopore and the single analyte molecule (Fig. 1d). Signals observed when testing the purified monomer fractions were long dwell time, full current blockades with occasional bumping events mixed in (Figure S2a). The bumping events observed in the monomer fraction can be attributed to the fact that Aβ40 monomer begins immediate aggregation upon elution from SEC [29]. Within 1 h, aggregation in the monomer fraction is inevitable [30]. After a 24-h incubation to promote more aggregation, significantly fewer monomer events and a larger relative number of bumping events were detected by nanopore (Figure S2b). Conversely, when testing the large soluble aggregate species eluted within SEC void volume, virtually absent were long dwell time, full current blockades characteristic of monomer translocation – only brief, small blockade events characteristic of species too large to transit the pore were observed (Figure S2c).

### 2.2. Quantitative characterizations of nanopore reference signals

To verify the existence and purity of Aβ40 monomer, oligomer, and large soluble aggregate molecular species in each reference sample, dynamic light scattering (DLS) analysis was performed (Fig. 2a-c). DLS scan of freshly purified monomers depicts a gaussian distributed peak centered at 0.6 nm (Fig. 2a). A downfield shift of the parent gaussian peak centered at 1.0 nm and the evolution of a second, more downfield peak centered at 8 nm are observed after a 24-h incubation, which confirms the presence of oligomers (Fig. 2b) [28]. DLS scan of Aβ40 large soluble aggregates from SEC void volume displayed a single, large gaussian peak centered at 100 nm (Fig. 2c). To quantify each species, scatter plots of current blockade (I/I<sub>0</sub>) against dwell time (ms) were established for all valid signal peaks on their nanopore sensorgrams. An abundance of full translocation signals (long dwell times and full current blockades) and bumping signals (short dwell times and partial current blockades) were observed for both purified monomer and 24-h incubated samples due to the immutable oligomerization process (Fig. 2d and e), whereas the large soluble aggregate scatter plot only depicts bumping events exclusively (Fig. 2f). Histograms of relative event frequency versus current blockade and dwell time can further elucidate distinctions in signal characteristics of these molecular species. We observed an overall shift in relative event frequency (abundance) of total current blockades characteristic of monomers (I/I<sub>0</sub>: 0.8–1.0) (Fig. 2g), to a mix of monomer events and increasing oligomer bumping events (Fig. 2h), and finally to partial current blockades characteristic of oligomers and large soluble aggregates (I/I<sub>0</sub>: 0.25-0.35) (Fig. 2i). A similar changing trend is observed for dwell time where relative event frequency for long dwell time events decreases as sampling moves from monomers (Fig. 2j) to oligomers (Fig. 2k) to large soluble aggregates (Fig. 21). Reproducibility of the nanopore biosensor was confirmed by

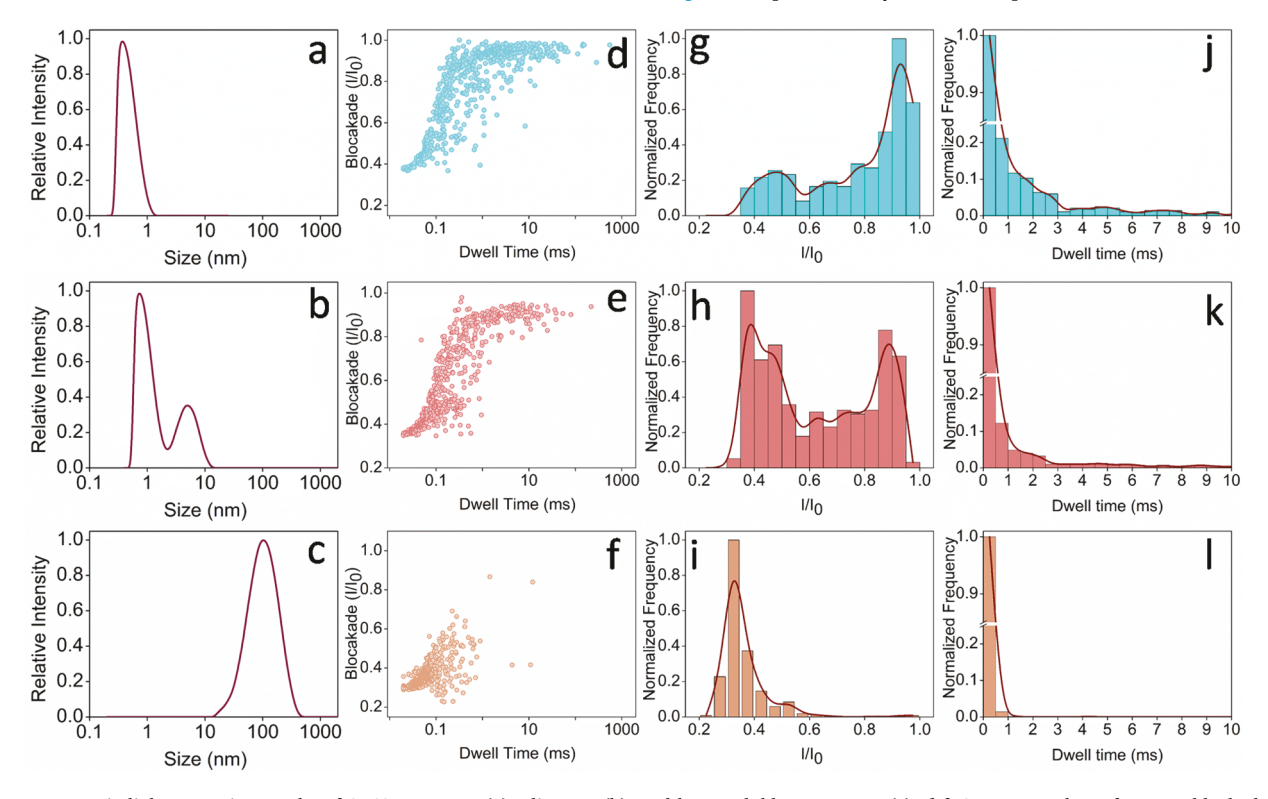


Fig. 2. a-c: Dynamic light scattering results of Aβ40 monomer (a), oligomer (b), and large soluble aggregates (c). d-f: 2D scatter plots of current blockade versus dwell time of valid events from nanopore results of Aβ40 monomer (d), oligomer (e), and large soluble aggregates (f). g-i: Histograms of normalized event frequency versus current blockade for Aβ40 monomer (g), oligomer (h), and large soluble aggregates (i). j-l: Histograms of normalized event frequency versus dwell time for Aβ40 monomer (j), oligomer (k), and large soluble aggregates (l).

results from three different nanopores including >500 individual sensing events per run (Figure S3). As confirmed with DLS analysis, these nanopore results established quantitative profiles of A $\beta$ 40 monomers (~0.6 nm), oligomers (~8 nm), and large soluble aggregates (~100 nm) based on their sizes, which are fundamental to studying A $\beta$ 40 peptide aggregation dynamics.

# 2.3. Temperature dependent aggregation dynamics at the single-molecule level

To probe its aggregation dynamics, freshly purified A $\beta$ 40 monomers were incubated at both 4 °C and 37 °C and sampled by the nanopore biosensor over a 20-day period. A qualitative comparison between the 2D kernel density scatter plots (current blockade vs. dwell time) of the aggregating monomers at 4 °C (Fig. 3a) and at 37 °C (Fig. 3b) reveals a vacillation between relatively high and relatively low monomer events in the early aggregation time points that is followed by, at later time points, a more complete and stable state of aggregation. Further deduction from this qualitative comparison of the scatter density plots

leads one to immediately recognize that the monomer aggregation at 37 °C is not only more complete but also occurs faster than at 4 °C, which can be attributed to the fact that aggregation dynamics and molecular encounterings in solution are largely governed by temperature [31]. Quantitative analysis of relative monomer and oligomer event frequencies at each time point depict the overall trend of Aβ40 aggregation dynamics at 4 °C and 37 °C (Fig. 3c&d, S4, and S5). A monomer event is defined as having a current blockade value ranging from 0.8 to 1.0, while an oligomer event is defined by current blockade between 0.3 and 0.6. Both monomer and oligomer event frequencies at  $4\,^{\circ}\text{C}$  and  $37\,^{\circ}\text{C}$ were fit with 2nd power polynomial. Observed in the early time points is an oscillating above and below the fitting line and can be described by the solution approaching a dynamic equilibrium that it continually over and under shoots along the aggregation pathway. We anticipate this observed oscillation can be further explained by the fact that high energy, unstable, off-pathway oligomers are formed [32-38], and that these off-pathway oligomers reorder continuously along the aggregation pathway, liberating and absorbing free floating monomers in large numbers as the more favorable, lower energy, highly ordered large

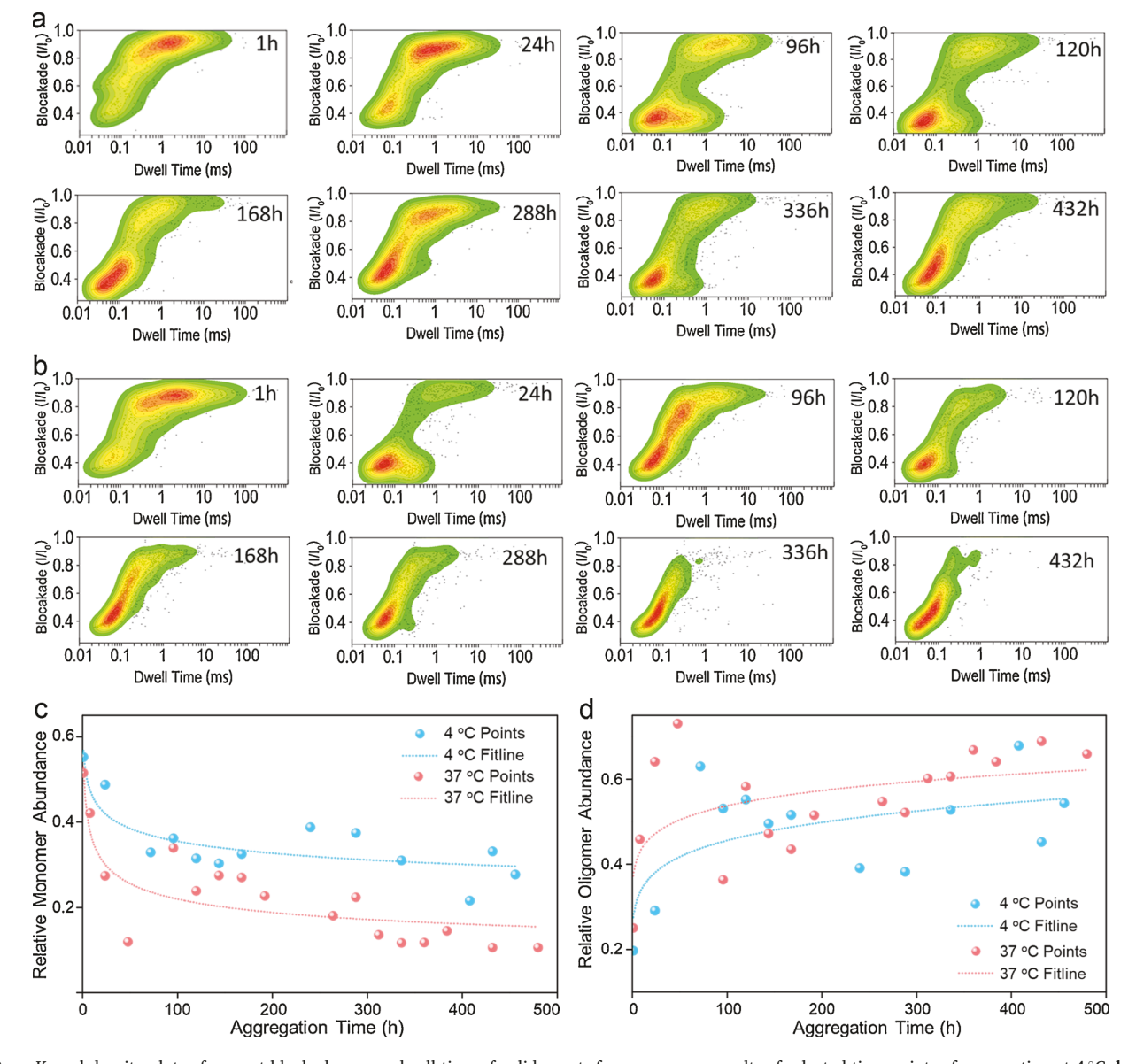


**Fig. 3. a:** Kernel density plots of current blockade versus dwell time of valid events from nanopore results of selected time points of aggregation at 4 °C. **b:** Kernel density plots of current blockade versus dwell time of valid events from nanopore results of selected time points of aggregation at 37 °C. **c:** Relative monomer abundance versus aggregation time. The total number of monomer/oligomer events was divided by the total number of all events to calculate the relative abundance.

soluble aggregate and fibril structures are spontaneously yielded [4,9, 39–44]. Eventually, aggregation plateaus were observed under both temperatures. The sample aggregating at 37  $^{\circ}$ C undergoes a more complete and stable aggregation, while the 4  $^{\circ}$ C sample in dynamic equilibrium has much more free-floating monomer available in solution.

### 3. Conclusion

This work demonstrates the proof-of-concept of a biological nanopore as a dynamic peptide aggregation biosensor at the single-molecule level. AD symptoms are thought to begin early in one's life and progress as the individual senesces - hence, understanding early aggregation of Aß peptides that correlate with the state of AD development is highly desirable. The benefit of using single molecule biosensors like the  $\alpha HL$ nanopore lies in its ultra-sensitivity to conformational changes of analytes. Due to the simplicity, robustness, reproducibility, and costefficiency in system configuration, as well as similarity of cell chemistry in the sensing environment, nanopore biosensors open up new possibilities for in-depth studies of  $A\beta$  aggregation that other common analytical chemistry technologies like ELISA, mass spectrometry, and HPLC may miss. However, for future clinical applications, immunoprecipitation is necessary to separate AB peptides and aggregates from clinical specimens, as nanopores only have moderate selectivity and may foul due to other biomolecules in the specimen. Our future work involves: (1) expanding the current work towards utilizing the nanopore system as a drug screening device to study influences of small molecule drugs to the aggregation dynamics for possible AD therapeutics; (2) detecting low concentration AD biomarkers that can be extracted from common body fluids like blood, urine, and cerebrospinal fluid to inform early diagnosis.

### CRediT authorship contribution statement

Brian Lenhart: Conceptualization, Methodology, Investigation, Formal analysis, Writing - original draft. Xiaojun Wei: Methodology, Formal analysis, Visualization. Brittany Watson: Methodology, Investigation. Xiaoqin Wang: Methodology, Formal analysis. Zehui Zhang: Methodology, Formal analysis. Chen-zhong Li: Methodology, Formal analysis. Welissa Moss: Conceptualization, Resources, Formal analysis, Writing - review & editing. Chang Liu: Conceptualization, Funding acquisition, Resources, Supervision, Methodology, Formal analysis, Writing - review & editing.

# **Declaration of Competing Interest**

The authors report no declarations of interest.

## Acknowledgements

C. Liu acknowledges the financial support from the National Institute of Allergy and Infectious Diseases (NIAID) award K22AI136686, the South Carolina IDeA Networks of Biomedical Research Excellence Developmental Research Project by the National Institute of General Medical Sciences (NIGMS) award P20GM103499, and the National Science Foundation (NSF) CAREER Award 2047503.

### Appendix A. Supplementary data

Supplementary material related to this article can be found, in the online version, at doi:https://doi.org/10.1016/j.snb.2021.129863.

### References

 N.E. Pryor, M.A. Moss, C.N. Hestekin, Unraveling the early events of amyloid-beta protein (Abeta) aggregation: techniques for the determination of Abeta aggregate size, Int. J. Mol. Sci. 13 (3) (2012) 3038–3072.

- [2] K.G. Mawuenyega, et al., Amyloid-beta isoform metabolism quantitation by stable isotope-labeled kinetics, Anal. Biochem. 440 (1) (2013) 56–62.
- [3] A. Nakamura, et al., High performance plasma amyloid-beta biomarkers for Alzheimer's disease, Nature 554 (7691) (2018) 249–254.
- [4] D.D. Soto-Ortega, et al., Inhibition of amyloid-beta aggregation by coumarin analogs can be manipulated by functionalization of the aromatic center, Bioorg. Med. Chem. 19 (8) (2011) 2596–2602.
- [5] J. Houghtaling, J. List, M. Mayer, Nanopore-based, rapid characterization of individual amyloid particles in solution: concepts, challenges, and prospects, Small 14 (46) (2018) e1802412.
- [6] I.G. McKeith, Consensus guidelines for the clinical and pathologic diagnosis of dementia with Lewy bodies (DLB): report of the consortium on DLB International workshop, J. Alzheimers Dis. 9 (3 Suppl) (2006) 417–423.
- [7] N. Sharma, A.N. Singh, Exploring biomarkers for Alzheimer's disease, J Clin Diagn Res 10 (7) (2016) KE01–6.
- [8] A. Sanabria-Castro, I. Alvarado-Echeverria, C. Monge-Bonilla, Molecular pathogenesis of Alzheimer's disease: an update, Ann Neurosci 24 (1) (2017) 46–54.
- [9] M.R. Nichols, et al., Amyloid-beta protofibrils differ from amyloid-beta aggregates induced in dilute hexafluoroisopropanol in stability and morphology, J. Biol. Chem. 280 (4) (2005) 2471–2480.
- [10] F.J. Gonzalez-Velasquez, J.A. Kotarek, M.A. Moss, Soluble aggregates of the amyloid-beta protein selectively stimulate permeability in human brain microvascular endothelial monolayers, J. Neurochem. 107 (2) (2008) 466–477.
- [11] J.W.F. Robertson, J.E. Reiner, The utility of nanopore technology for protein and peptide sensing, Proteomics 18 (18) (2018) e1800026.
- [12] K. Lee, et al., Recent progress in solid-State nanopores, Adv. Mater. 30 (42) (2018) e1704680.
- [13] J. Wilson, et al., Graphene nanopores for protein sequencing, Adv. Funct. Mater. 26 (27) (2016) 4830–4838.
- [14] J.J. Kasianowicz, et al., Nanoscopic porous sensors, Annu Rev Anal Chem (Palo Alto Calif) 1 (2008) 737–766.
- [15] S. Howorka, H. Bayley, Probing distance and electrical potential within a protein pore with tethered DNA, Biophys. J. 83 (6) (2002) 3202–3210.
- [16] C. Plesa, N. van Loo, C. Dekker, DNA nanopore translocation in glutamate solutions, Nanoscale 7 (32) (2015) 13605–13609.
- [17] X. Wei, et al., Enabling nanopore technology for sensing individual amino acids by a derivatization strategy, J. Mater. Chem. B 8 (31) (2020) 6792–6797.
- [18] X. Wei, et al., N-terminal derivatization-assisted identification of individual amino acids using a biological nanopore sensor, ACS Sens 5 (6) (2020) 1707–1716.
- [19] G. Gibrat, et al., Polyelectrolyte entry and transport through an asymmetric alphahemolysin channel, J. Phys. Chem. B 112 (47) (2008) 14687–14691.
- [20] B. Lenhart, et al., Nanopore fabrication and application as biosensors in neurodegenerative diseases, Crit. Rev. Biomed. Eng. 48 (1) (2020) 29–62.
- [21] A. Asandei, et al., Placement of oppositely charged aminoacids at a polypeptide termini determines the voltage-controlled braking of polymer transport through nanometer-scale pores, Sci. Rep. 5 (2015) 10419.
- [22] A.R. Hall, et al., Hybrid pore formation by directed insertion of alpha-haemolysin into solid-state nanopores, Nat. Nanotechnol. 5 (12) (2010) 874–877.
- [23] T. Luhrs, et al., 3D structure of Alzheimer's amyloid-beta(1-42) fibrils, Proc Natl Acad Sci U S A 102 (48) (2005) 17342–17347.
- [24] H. Bayley, Single-molecule DNA sequencing getting to the bottom of the well, Nat. Nanotechnol. 12 (12) (2017) 1116–1117.
- [25] H.Y. Wang, et al., Nanopore analysis of beta-amyloid peptide aggregation transition induced by small molecules, Anal. Chem. 83 (5) (2011) 1746–1752.
- [26] R.-J. Yu, et al., Single molecule sensing of amyloid-β aggregation by confined glass nanopores, Chem. Sci. 10 (46) (2019) 10728–10732.
- [27] R. Cukalevski, et al., The A beta 40 and A beta 42 peptides self-assemble into separate homomolecular fibrils in binary mixtures but cross-react during primary nucleation, Chem. Sci. 6 (7) (2015) 4215–4233.
- [28] G. Bitan, et al., Amyloid beta -protein (Abeta) assembly: Abeta 40 and Abeta 42 oligomerize through distinct pathways, Proc Natl Acad Sci U S A 100 (1) (2003) 330–335.
- [29] F. Gonzalez-Velasquez, et al., Activation of brain endothelium by soluble aggregates of the amyloid-beta protein involves nuclear factor-kappaB, Curr Alzheimer Res 8 (1) (2011) 81–94.
- [30] X. Li, et al., Label-free detection of early oligomerization of alpha-synuclein and its mutants A30P/E46K through solid-state nanopores, Nanoscale 11 (13) (2019) 6480–6488.
- [31] V. Vetri, et al., Fluctuation methods to study protein aggregation in live cells: concanavalin a oligomers formation, Biophys. J. 100 (3) (2011) 774–783.
- [32] T.P. Knowles, et al., Kinetics and thermodynamics of amyloid formation from direct measurements of fluctuations in fibril mass, Proc Natl Acad Sci U S A 104 (24) (2007) 10016–10021.
- [33] A. Baumketner, et al., Amyloid beta-protein monomer structure: a computational and experimental study, Protein Sci. 15 (3) (2006) 420–428.
- [34] S.L. Bernstein, et al., Amyloid beta-protein: monomer structure and early aggregation states of Abeta42 and its Pro19 alloform, J. Am. Chem. Soc. 127 (7) (2005) 2075–2084.
- [35] B. O'Nuallain, et al., Seeding specificity in amyloid growth induced by heterologous fibrils, J. Biol. Chem. 279 (17) (2004) 17490–17499.
- [36] Z.C. Zhang, Y.M. Chook, Structural and energetic basis of ALS-causing mutations in the atypical proline-tyrosine nuclear localization signal of the fused in sarcoma protein (FUS), Proc. Natl. Acad. Sci. U. S. A. 109 (30) (2012) 12017–12021.
- [37] A. Laganowsky, et al., Atomic view of a toxic amyloid small oligomer, Science 335 (6073) (2012) 1228–1231.

- [38] C.G. Glabe, Structural classification of toxic amyloid oligomers, J. Biol. Chem. 283 (44) (2008) 29639–29643.
- [39] J. Bieschke, et al., Small-molecule conversion of toxic oligomers to nontoxic betasheet-rich amyloid fibrils, Nat. Chem. Biol. 8 (1) (2011) 93–101.
- [40] W.L. Klein, G.A. Krafft, C.E. Finch, Targeting small Abeta oligomers: the solution to an Alzheimer's disease conundrum? Trends Neurosci. 24 (4) (2001) 219–224.
- [41] F.J. Gonzalez-Velasquez, et al., Soluble amyloid-beta protein aggregates induce nuclear factor-kappa B mediated upregulation of adhesion molecule expression to stimulate brain endothelium for monocyte adhesion, J. Adhes. Sci. Technol. 24 (13-14) (2010) 2105–2126.
- [42] T.J. Davis, et al., Comparative study of inhibition at multiple stages of amyloid-beta self-assembly provides mechanistic insight, Mol. Pharmacol. 76 (2) (2009) 405–413.
- [43] M.R. Nichols, et al., Amyloid-beta aggregates formed at polar-nonpolar interfaces differ from amyloid-beta protofibrils produced in aqueous buffers, Microsc. Res. Tech. 67 (3-4) (2005) 164–174.
- [44] M.R. Nichols, et al., Growth of beta-amyloid(1-40) protofibrils by monomer elongation and lateral association. Characterization of distinct products by light scattering and atomic force microscopy, Biochemistry 41 (19) (2002) 6115–6127.